

This document is confidential and is proprietary to the American Chemical Society and its authors. Do not copy or disclose without written permission. If you have received this item in error, notify the sender and delete all copies.

**Graphene-Oxide Functionalized with 2-Ureido-4[1H]-pyrimidinone for Production of Nacre-Like Films**

Journal:	<i>ACS Applied Nano Materials</i>
Manuscript ID	an-2020-01488s.R2
Manuscript Type:	Article
Date Submitted by the Author:	05-Jun-2020
Complete List of Authors:	Smith, Andrew; University of Warwick Kelly, Nicole; University of Warwick Figiel, Lukasz; University of Warwick Wan, Chaoying; University of Warwick, International Manufacturing Centre Hanna, John; University of Warwick, Department of Physics Farris, Stefano; Universita degli Studi di Milano, DeFENS - Food, Environmental and Nutritional Sciences McNally, Tony; University of Warwick, Institute for Nanocomposite Manufacturing

SCHOLARONE™  
Manuscripts

# Graphene-Oxide Functionalized with 2-Ureido-4[1*H*]-pyrimidinone for Production of Nacre-Like Films

Andrew J. Smith,<sup>1</sup> Nicole L. Kelly,<sup>2</sup> Łukasz Figiel,<sup>1</sup> Chaoying Wan,<sup>1</sup> John V. Hanna,<sup>2</sup>

Stefano Farris<sup>3</sup>, Tony McNally\*<sup>1</sup>

<sup>1</sup>International Institute for Nanocomposites Manufacturing (IINM), WMG, and <sup>2</sup>Department of Physics, University of Warwick, Coventry, CV4 7AL, UK

<sup>3</sup>Department of Food, Environmental and Nutritional Sciences, University of Milan, 20133 Milano, Italy

Corresponding Author: t.mcnally@warwick.ac.uk

## Abstract

The facile and efficient reaction of graphene oxide (GO) and 2-Ureido-4[1*H*]-pyrimidinone (UPy), an isocyanate terminated 4-site hydrogen-bonding moiety, produces a functionalised GO (*f*-GO) that readily self-assembles into a freestanding nacre-like film using a vacuum filtration process. The reaction of UPy with GO occurs predominately via the epoxide and hydroxyl groups on the GO which was confirmed from a combination of Fourier-transform infrared (FTIR), Raman and X-ray photoelectron spectroscopy (XPS) and <sup>13</sup>C Solid State Nuclear Magnetic Resonance (SSNMR) measurements. The nacre-like films obtained were typically 50µm to 100µm thick, from cross-section scanning-electron microscopy (SEM) imaging. The GO *d*-spacing (X-ray diffraction, XRD) increased with increasing UPy content from 0.934nm to 1.45nm, resulting in porous films with reduced tortuosity to oxygen, carbon dioxide and water. However, at higher UPy content reduced tortuosity is, balanced with the ability of UPy dimers to readily dissociate and exchange with water. The tensile strength and tensile toughness of the GO nacre-like film increased by up to 470% and 1100% and the maximum strain by a factor of ~2, for the film with the highest UPy content. These

improvements are achieved through a mechanism of extension and unfolding of the linear chain of six carbon atoms in UPy, enhancing strain under tensile loading permitting the platelets to slide more before failure. This work highlights the impact of enhanced interlayer interactions via hydrogen bonding in producing polymer-free nacre-like films.

Keywords: Graphene-oxide, 2-Ureido-4[1H]-pyrimidinone, functionalisation, nacre-like films, mechanical properties, barrier properties

## 1. Introduction

Numerous approaches have been employed to functionalise graphene oxide (GO).<sup>1-3</sup> Of these methods the reaction of GO with isocyanates is arguably the most simplistic,<sup>4, 5</sup> as the reaction can be completed at room temperature within 24 hours, achieving the functionalised GO (*f*-GO) product in high yield. Despite the ease of the reaction, studies on the functionalisation of GO using this approach are few. This may be due to the hazardous nature of the isocyanate reagents, however post-reaction the amide, carbamate, and oxazolidone products are more benign. Through functionalisation the surface behaviour of GO can be tailored to achieve many desirable properties including improved dispersion in polymer matrices,<sup>1</sup> adsorption/capture of chemicals<sup>6</sup> and antifouling behaviour in filter membranes<sup>7</sup>.

Interest in the production and properties of nacre-mimetic materials (analogous to the shells of the mollusc family) has grown dramatically in recent years.<sup>8-11</sup> Typically, nacre-mimetic materials are constructed *via* a brickwork arrangement of a nanoplatelet based hard phase, infused with a soft, polymer phase that behaves like a glue. In nature, the nanoplatelet phase makes up at least 95% by volume of the material with the polymer phase providing the remaining 5%.<sup>12</sup> Synthetic equivalents have been successfully prepared with a wider range of polymer loadings. It is widely recognised that the cooperative effect of the soft and hard phase results in remarkable material properties through a range of energy dissipation processes.<sup>13, 14</sup>

GO is a popular choice as a hard phase due to its high mechanical strength, relative ease of dispersion in water and the favourable interactions possible with a range of polymer phases.<sup>15-18</sup> Resultant nacre-like films can also be readily reduced with hydriodic acid to greatly improve mechanical and electrical properties.<sup>18</sup> To date, the focus of research in this field has been towards optimising interactions between the polymer (glue) and nanoplatelet (brick). This has included targeted covalent<sup>8, 15</sup> and non-covalent<sup>17, 19</sup> crosslinking of GO through the polymer phase towards improved interfacial interactions and in turn an improvement in mechanical properties.

In this work, we report a direct functionalisation approach in which GO is treated with a 4-site hydrogen-bonding moiety (2-Ureido-4[1*H*]-pyrimidinone, UPy) *via* a simple isocyanate reaction (*f*-GO). The resultant *f*-GO was dispersed in dimethyl sulfoxide (DMSO) before undergoing vacuum filtration to produce nacre-like films. This work is, to the best of our knowledge, the first example of functionalisation of GO *via* this isocyanate treatment towards application as a nacre-like material. The initial reaction between GO and the UPy is confirmed from Fourier-transform infrared spectroscopy (FTIR), X-ray diffraction (XRD) and Raman spectroscopy and the degree of functionalisation studied using X-ray photoelectron (XPS) and <sup>13</sup>C solid state nuclear magnetic resonance (SSNMR) spectroscopy. The structure of the films was analysed with scanning-electron microscopy (SEM) and XRD and the tensile mechanical and barrier properties (oxygen, water and carbon dioxide) measured.

## 2. Experimental

### 2.1 Materials

GO was purchased from Abalonyx, Norway in powder form and used with no further purification. 2-amino-4-hydroxy-6-methylpyrimidine and DMF were purchased from Fisher Scientific and, hexamethylene diisocyanate (HDI) was purchased from VWR International.

Dichloromethane (DCM) and DMSO were purchased from Merck. All chemicals were used as received. Hydrophilic poly(tetrafluoroethylene) PTFE membranes were purchased from Merck.

## 2.2. Synthesis Methods

### 2.2.1. Synthesis of 2-Ureido-4[1*H*]-pyrimidinone (UPy)

2-amino-4-hydroxy-6-methylpyrimidine (4.38 g, 35.0 mmol) was combined with an excess of HDI (38.0 cm<sup>3</sup>, 237 mmol), and heated at 100 °C for 24 hours. A white precipitate formed and was filtered under vacuum. The resulting solid (Figure S1) was washed multiple times with *n*-pentane achieving a white powder in excellent yield (10.17 g, 34.7 mmol, 99%).

### 2.2.2. Reaction of UPy with GO

Functionalisation of GO with UPy was achieved using the method outlined by Stankovich *et al.*<sup>4</sup> Typically GO (≈1.5 g) was combined in solid form with UPy at a weight ratio of GO:UPy = 1:1, 1:0.1 and 1:0.01 and will be referred to as GO.UPy.50.50, GO.UPy.90.10 and GO.UPy.99.1, respectively. Anhydrous DMF (75 cm<sup>3</sup>) was added and the mixture degassed with N<sub>2</sub> for 1 hour, then stirred for 24 hours. The resultant dispersion was coagulated in DCM (≈200 cm<sup>3</sup>) filtered under vacuum and washed with DCM. The brown powder obtained was dried overnight at 40 °C under vacuum.

### 2.2.3. Production of GO.UPy films

GO.UPy films were produced using a vacuum filtration method in which GO.UPy (≈500 mg) was dispersed in DMSO (50 cm<sup>3</sup>). Numerous attempts were made with other solvents to prepare stable dispersions, see Table S1. The mixture was then stirred for 2 hours before being filtered through a hydrophilic PTFE membrane with a pore size of 0.22 μm. The films obtained (Figure S2) were dried overnight at 40 °C before being peeled from the membrane.

#### 2.2.4. Characterisation

Fourier-transform infrared (FTIR) spectra of all materials were recorded on a Bruker Spectrometer in a scan range from 500  $\text{cm}^{-1}$  to 4000  $\text{cm}^{-1}$ .

Scanning Electron Microscopy (SEM) micrographs were obtained using a Zeiss Sigma instrument using an InLens detector at 10kV. The samples imaged were sputter coated using an Au/Pd target.

Raman spectra were collected on a Renishaw inVia Raman microscope instrument, using a 532 nm laser in the wavenumber range 100  $\text{cm}^{-1}$  and 3200  $\text{cm}^{-1}$  with a 10-second exposure time, 15 accumulations with the laser power set at 10%.

X-ray Photoelectron Spectroscopy (XPS) was carried out using a Kratos Axis Ultra DLD Spectrometer at RT and with a base pressure of  $2 \times 10^{-10}$  mbar, using a monochromated Al  $k_{\alpha}$  X-ray source. In order to prevent surface charging the data was collected while the sample was exposed to a flux of low energy electrons from the charge neutralizer built in to the hemispherical analyser entrance, with the binding energy scale retrospectively calibrated to the  $\text{sp}^3$  C-C peak at 284.6 eV. The data was analysed with CasaXPS software, using Shirley backgrounds and mixed Gaussian-Lorentzian (Voigt) line shapes and asymmetry parameters where appropriate. For compositional analysis, the analyser transmission function was determined using clean metallic foils to determine the detection efficiency across the full binding energy range.

XRD measurements were performed on a 3<sup>rd</sup> generation Malvern Panalytical Empyrean instrument equipped with multicore (iCore/dCore) optics and a Pixcel3D detector operating in 1D scanning mode. A Cu tube was utilised giving Cu  $K_{\alpha 1/2}$  radiation (1.5419 Å) and a beam knife to reduce air scatter at the low angles. Scans were recorded in the range  $4^{\circ}$  to  $30^{\circ}$   $2\theta$  with a step size of  $0.0263^{\circ}$  and a counting time of  $\sim 130$  s/step. Using the measured diffraction angle,

2 $\theta$ , the interlayer spacing ( $d$ ) was calculated using Bragg's Law,  $n\lambda = 2d\sin\theta$  (where  $\lambda = 1.541$  Å).

Tensile testing was completed using an Instron 5800R machine equipped with a 500N load cell and a loading rate controlled at 1 mm/min. Test specimens were cut into bars of width 10 mm and, length 40 mm using a razor blade. (Thicknesses were determined from cross-sectional SEM analysis and the average taken from 10 measurements). The RT tensile mechanical properties were determined from an average of at least five (5) specimens. The Young's modulus was calculated from the gradient of the linear region of the stress-strain curve and tensile toughness calculated from the area under the stress-strain curves.

All solid state nuclear magnetic resonance measurements were performed at 9.4 T using a Bruker Avance-400 spectrometer operating at  $^1\text{H}$  and  $^{13}\text{C}$  Larmor frequencies ( $\nu_0$ ) of 400.13 and 100.59 MHz, respectively. Single pulse  $^{13}\text{C}$  (direct detection) experiments facilitating a quantitative analysis of the carbon speciation were performed using a Bruker 4 mm HX probe which enabled a magic-angle-spinning (MAS) frequency of 12 KHz to be implemented. Pulse length calibration was performed using solid alanine from which a  $\pi/2$  pulse time of 3  $\mu\text{s}$  was measured. All  $^{13}\text{C}$  MAS NMR experiments were implemented using a  $\pi/2$  nutation angle and a relaxation delay of 60 s between excitation pulses. For all experiments, 100 kHz of  $^1\text{H}$  decoupling was applied during, the acquisition of all FIDs. All  $^{13}\text{C}$  chemical shifts were externally referenced against the IUPAC recommended primary reference of  $\text{Me}_4\text{Si}$  (1 % in  $\text{CDCl}_3$ ,  $\delta = 0.0$  ppm), via the secondary solid alanine reference ( $\delta = 20.5$  ppm).<sup>20</sup>

The gas (oxygen and carbon dioxide) and water vapour barrier properties of the films were assessed using a Totalperm permeability analyzer (Extrasolution Srl, Pieve Fosciana, Italy) equipped with both an electrochemical sensor (for oxygen) and an infrared sensor (for carbon dioxide and water vapour). Specimens of approximately 2 cm x 2 cm were sandwiched between two aluminium-tape masks, exposing a surface of 2.01  $\text{cm}^2$  for the permeation of the

gas/vapour molecules. The oxygen and carbon dioxide transmission rate ( $O_2TR$  and  $CO_2TR$ ) in  $cm^3 m^{-2} 24h^{-1}$ ) were determined according to ASTM FD3985 and ASTM F2476, at  $23^\circ C$  and 0% relative humidity (RH). Water vapour transmission rate (WVTR, expressed in  $g m^{-2} 24h^{-1}$ ) was determined according to ASTM F1249 at  $38^\circ C$  and 90% RH. All the tests were carried out with a carrier flow ( $N_2$ ) of  $10 mL min^{-1}$  and at 1 atm partial pressure difference (for  $O_2$  and  $CO_2$ ) and, 59.04 mbar vapour partial pressure difference (for WVTR) on the two sides of the specimen. To reset any difference in the transmission rate (TR) values possibly arising from different thicknesses, TR values were used to determine a permeability coefficient ( $P'O_2$ ,  $P'CO_2$  and  $P'WV$ ) using the following equation:

$$P'G = PG \times t = \frac{GTR}{\Delta p} \times t \quad (1)$$

where,  $P'G$  is the gas (or vapour) permeability coefficient ( $cm^3 mm m^{-2} 24h^{-1} atm^{-1}$ ),  $PG$ , is the permeance (defined as the ratio of the  $GTR$  to the difference between the partial pressure of the gas on the two sides of the film,  $Dp$ ), and  $t$  is the total thickness of the material.

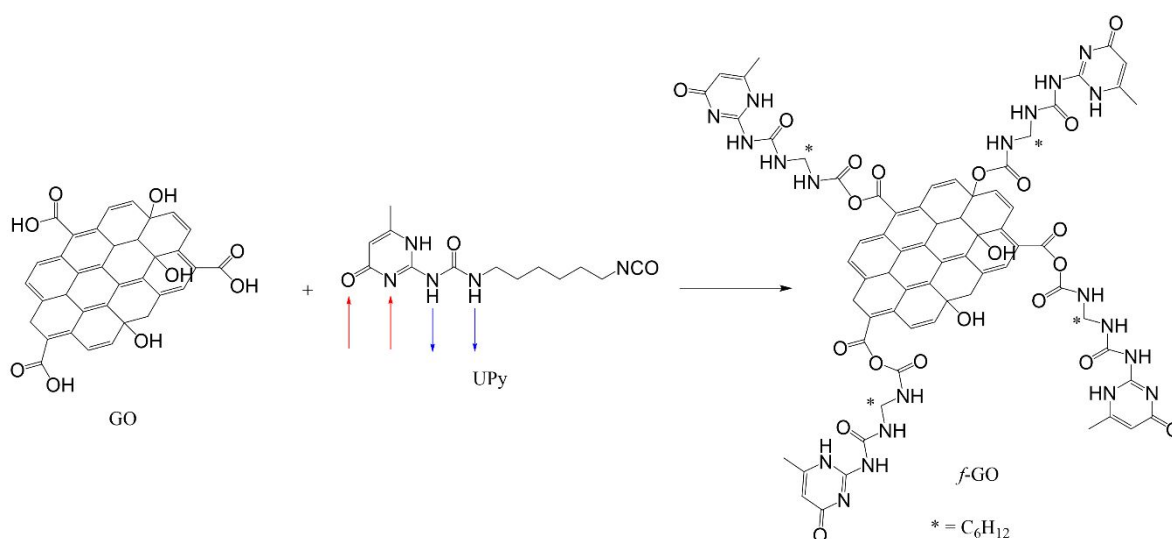
### 3. Results and Discussion

The surface of GO has a relatively high abundance of functional groups that can be used for chemical reactions.<sup>21</sup> The simple and effective reaction of the carboxylic acid, hydroxyl and epoxide groups present on the surface of GO with a free isocyanate is exploited to achieve surface functionalised GO. The reaction of a carboxylic acid and an isocyanate has been known for many years<sup>22</sup> and proceeds *via* a condensation reaction in which  $CO_2$  is released.<sup>22, 23</sup> The initial step of the reaction proceeds through an attack of the carboxylate ion on the electropositive sp carbon of the isocyanate group. Following this, the anhydride intermediate produced undergoes an intramolecular rearrangement to expel  $CO_2$ . This ultimately forms an amide species that is detectable by FTIR. Theoretically, the hydroxyl and epoxide groups of GO can also undergo a similar attack of the isocyanate carbon that results in a carbamate



species and an oxazolidone.<sup>24</sup> Example mechanisms are available in the supporting information (Scheme S1).

The reactivity between the aromatic and aliphatic carboxylic acids and isocyanates has been shown to be less for the aromatic species.<sup>22</sup> The functional groups used for this reaction are close to  $sp^2$  carbons, where the graphene-like structure has been oxidised to form  $sp^3$  hybridisation and therefore has lost much of its aromaticity. As a result, a successful and rapid reaction occurred at room temperature within 24 hours (Scheme 1). This is confirmed from the FTIR spectra recorded (Figure 1 a)). GO displays two key peaks between 1000 and 2000  $cm^{-1}$ , one at 1618  $cm^{-1}$  corresponding to the O-H bend of trapped water and the other at 1722  $cm^{-1}$  which can be assigned to the C=O stretching of carboxylic acid and ketonic groups.<sup>25</sup> New peaks are observed following the reaction with the isocyanate and can be assigned to amide and carbamate groups at 1643  $cm^{-1}$  and 1560  $cm^{-1}$  produced *via* the reaction outlined in scheme 1. The peak at 1643  $cm^{-1}$  corresponds to an amide-carbonyl stretching vibration, otherwise referred to as the Amide-I vibrational stretch. The shoulder observed at 1560  $cm^{-1}$  can be assigned to the coupling of a C-N stretch with the CNH deformation vibration with an amide (known as the Amide-II vibration) but can also be observed in carbamate esters.<sup>4</sup>



**Scheme 1.** Reaction mechanism for functionalisation of GO with the 4-fold hydrogen-bonding group, UPy. The hydrogen-bonding sites are displayed as arrows on the UPy structure where, red = acceptor sites and blue = donor sites.

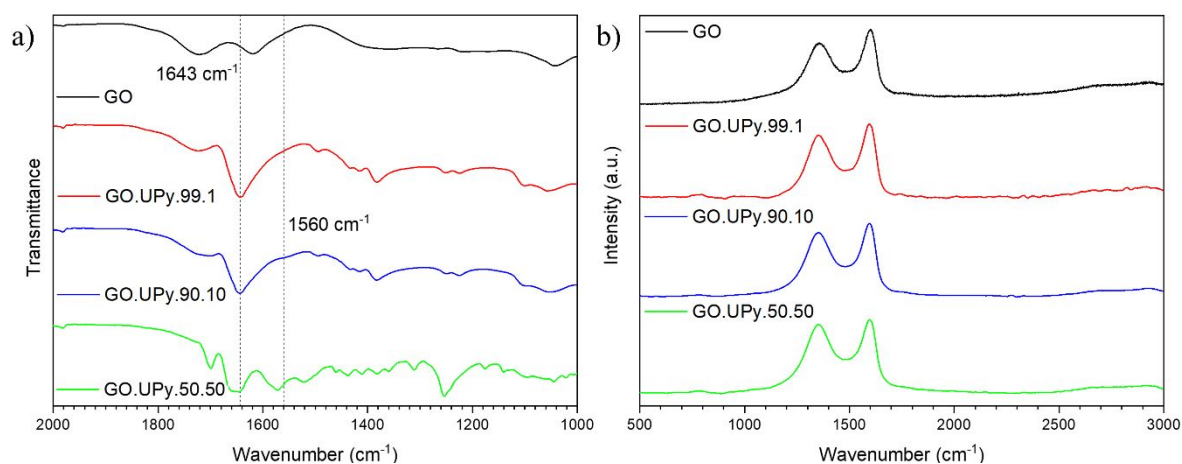


**Figure 1.** a) FTIR spectra of GO and GO.UPy between 2000  $\text{cm}^{-1}$  and 1000  $\text{cm}^{-1}$  and b) Raman spectra of GO and GO.UPy between 500  $\text{cm}^{-1}$  and 3000  $\text{cm}^{-1}$ .

The Raman spectra of the GO based materials displays two main peaks at approximately 1355  $\text{cm}^{-1}$  (D band), and close to 1600  $\text{cm}^{-1}$  (G band). The D band corresponds to an in-plane vibration of  $\text{sp}^2$  carbons in close proximity to a  $\text{sp}^3$  region. The G band is a primary in-plane vibration assigned to pristine  $\text{sp}^2$  domains.<sup>26</sup> Determining the ratio of the intensity of these two peaks ( $I_D/I_G$ ) provides information on the concentration of defects present within the GO material. A change in intensity of the D and G bands of the GO post-functionalisation is obtained, see Figure 1 b). On addition of the UPy (isocyanate), the  $I_D/I_G$  ratio increases, see Table 1. This is representative of an increase in the  $\text{sp}^3$  domain within the GO. The change in intensity ratio observed is relatively small and so suggests the functionalisation has a minimal effect on the structure of the GO. This is expected due to the reaction sites being carboxylic acid, hydroxyl and epoxide groups that are already present in defect-rich domains. The change

observed is however significant and provides further evidence for successful chemical modification of the surface of the GO.

**Table 1.**  $I_D/I_G$  ratios for GO and GO.UPy materials

Sample	GO	GO:UPy.99.1	GO:UPy.90.10	GO:UPy.50.50
D band ( $\text{cm}^{-1}$ )	1355	1354	1353	1352
G band ( $\text{cm}^{-1}$ )	1600	1597	1597	1597
$I_D/I_G$ ratio	0.848	0.874	0.871	0.919

XRD was performed to determine changes in the interlayer spacing within the GO and GO.UPy powder samples (Figure 2 a)). The dominant peak in the neat GO spectrum at  $2\theta = 10.84$  corresponds to a  $d$  spacing of 0.816 nm. Following reaction with UPy, this peak shifts towards lower  $2\theta$  values, i.e. larger  $d$ -spacing. Addition of increasing concentration of UPy results in a corresponding increase in the interlayer spacing, up to 1.144 nm for GO.UPy.50.50. This shift in  $2\theta$  and increase in  $d$ -spacing supports successful grafting of UPy onto GO.

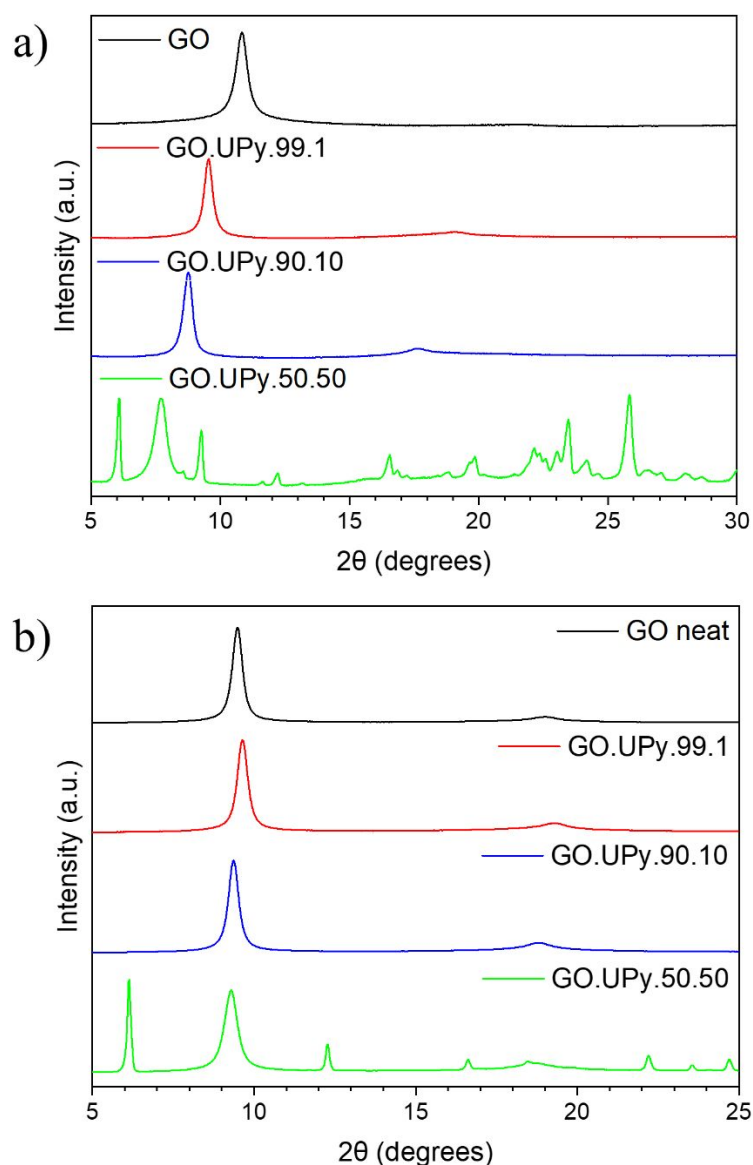


**Figure 2.** XRD diffractograms of GO and GO.UPy samples, a) in as synthesized powder form and b) as nacre-like films.

Single pulse  $^{13}\text{C}$  MAS NMR measurements were also used to confirm the functionalisation of GO with the isocyanate group. The  $^{13}\text{C}$  MAS NMR data from unreacted GO (see Figure 3 a)) shows characteristic resonances for surface terminated oxygen functional groups including epoxide ( $\delta = 61.8$  ppm), hydroxyl ( $\delta_{\text{iso}} = 70.2$  ppm) and carbonyl groups ( $\delta_{\text{iso}} = 166.1$  ppm). The  $\text{sp}^2$  graphitic region can also be observed as a broad peak centring at  $\delta_{\text{iso}} = 121.4$  ppm (Table S3). The assignment of these resonances has been established in previously

1  
2  
3 reported studies.<sup>27, 28</sup> Following functionalisation with UPy, evolution of new resonances in  
4  
5 addition to those ascribed to unreacted GO are observed (see Figures 3 b) - d)). These new  
6  
7 resonances appear at chemical shifts of  $\delta = 31.8$  ppm and 37.5 - 39.1 ppm, and can be assigned  
8  
9 to carbon species within the six-membered UPy group. In the spectra for the GO.UPy.50.50  
10  
11 samples, a further seven resonances are observed. It is likely these peaks are not observed in  
12  
13 GO.UPy.99.1 and GO.UPy.90.10 as the concentration of UPy in both of these samples is too  
14  
15 small to resolve the carbon environments. This could also be due to unreacted UPy adsorbed  
16  
17 to the GO surface as suggested from the XPS analysis.  
18  
19  
20  
21

22  
23 As observed from Figure 3, the intensity of the GO hydroxyl and epoxide resonances  
24  
25 decrease upon functionalisation with UPy. The intensity for epoxide resonance at  $\delta = 60.9$  -  
26  
27 61.8 ppm decreases monotonically 13.4, 12.0, 6.1 and 4.1 % as measured from the GO,  
28  
29 GO.UPy.99.1, GO.UPy.90.10 and GO.UPy.50.50 systems, respectively. Although the trend for  
30  
31 the hydroxyl groups at  $\delta = 70.2$  - 71.0 ppm is observed to initially increase in intensity when  
32  
33 comparing the unreacted GO to the GO.UPy.99.1 preparations, the subsequent trend for this  
34  
35 species decreases from 7.4% to 5.9% to 3.4% with increasing UPy incorporation in the reaction  
36  
37 mixture. These findings confirm that the isocyanate groups readily react with both the epoxide  
38  
39 hydroxyl species on the GO surface; however, it should be noted there is no apparent resonance  
40  
41 intensity trend measured from the carbonyl resonance located at  $\delta = 131.7$  - 132.0 ppm. The  
42  
43 predominance of the UPy reactivity with the surface hydroxyl and epoxide species on the  
44  
45 unreacted GO surface, with minimal affinity towards the carboxyl moieties, corroborates the  
46  
47 reaction mechanism outlined in Scheme S1 where the carboxylic acid group must be converted  
48  
49 to a carboxylate ion before reaction with isocyanate can occur.<sup>22</sup> Due to the acidic nature of the  
50  
51 GO surface, it is expected that the protonated carboxylic acid will dominate within the reaction  
52  
53 media, thus blocking the reaction from proceeding. An acidic environment is unlikely to have  
54  
55  
56  
57  
58  
59  
60

a negative impact on the reactivity of hydroxyl and epoxide groups and therefore, the UPy groups react more readily with these groups.

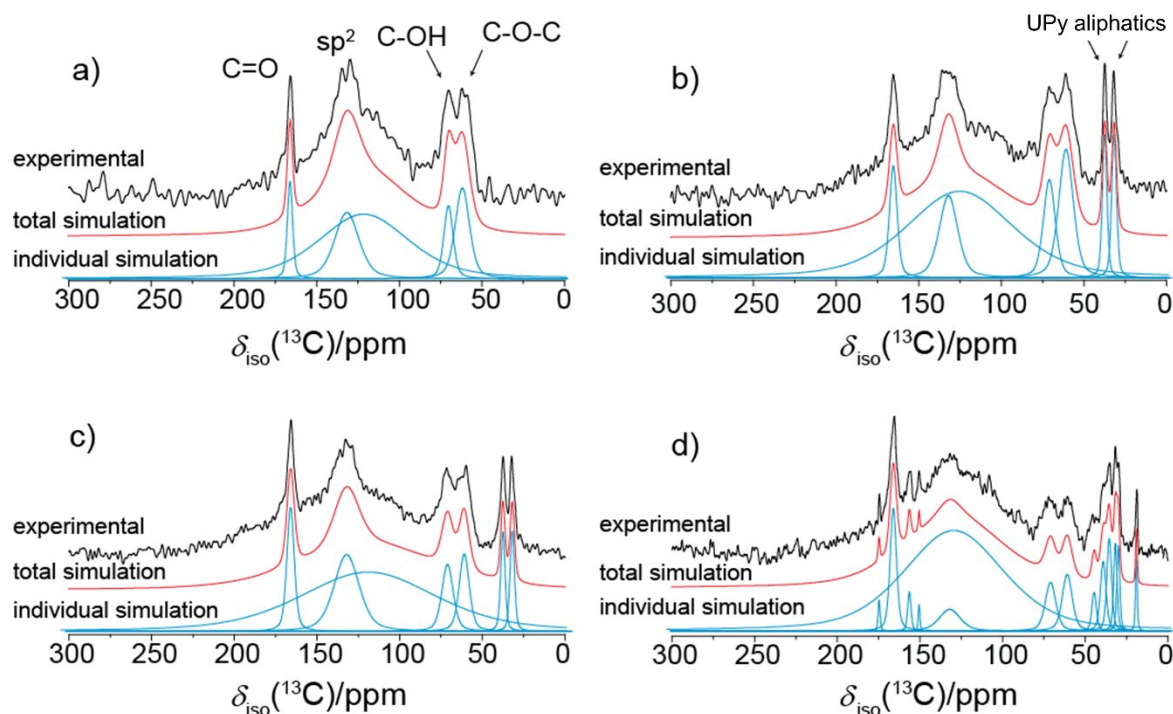


**Figure 3.** Solid state  $^{13}\text{C}$  MAS NMR data acquired from the a) unreacted GO, b) GO.UPy.99.1, c) GO.UPy.90.10 and d) GO.UPy.50.50 sample.

XPS analysis of the GO reveals only carbon and oxygen signals with trace amounts of sulphur and chlorine (the latter likely a result of reagents used in the synthesis of the GO nanoplatelets). The nitrogen content determined by this method is 0% as expected for neat GO. Following the reaction of GO with UPy, the elemental composition of the products is found to contain nitrogen (Table S1). The nitrogen content also increases with higher isocyanate loading, which would be expected in the case of successful grafting of the isocyanate groups to the GO surface and, can be observed in the XPS survey (Figure 4a)) by the appearance of the  $\text{N}_{1s}$  peak ( $\approx 400$  eV). From the de-convoluted spectra (Figure 4 b)-f)), the  $\text{C}_{1s}$  spectrum of

neat GO shows four peaks that can be attributed to binding energies for C-C (284.5 eV), C-O (286.4 eV), C=O (287.2 eV) and O=C-O (288.5 eV). Following the reaction with UPy, the C<sub>1s</sub> spectrum is de-convoluted into eight peaks with new peaks that are assigned to C-N (285.6 eV), O=C-N (288.1 eV) and N-(C=O)-N (290.1 eV). The C-C peak is also split into peaks for both the sp<sup>2</sup> (284.1 eV) and sp<sup>3</sup> (284.8 eV) domains. The development of these nitrogen-containing peaks confirms successful reaction of the UPy with GO. This is further supported by, the development of the N<sub>1s</sub> peak that is not present for neat GO. The N<sub>1s</sub> peak for both GO.UPy.99.1 and GO.UPy.90.10 can be de-convoluted into two peaks that can be assigned to C-N (399.8 and 400.2 eV) and N-H (401.3 and 401.7 eV) respectively.<sup>29</sup> In the case of GO.UPy.50.50, a third peak is detected that is attributed to C=N (399.0 eV). This is most likely a result of unreacted isocyanate adsorbing onto the GO surface through hydrogen bonding between the GO and the isocyanate molecule. On the assumption the C=N is derived from unreacted isocyanate, the C-N percentage can be corrected, providing a more accurate indication of the degree of functionalisation. The ratio of the intensity of the C-N and N-H peaks changes following addition of greater UPy content. The intensity of both peaks should increase but at an equal rate, the ratio of N-C to N-H increases. The high UPy content materials more readily form dimers via hydrogen bonding due to an increase in the availability of neighbouring UPy groups and following dimerization, the UPy groups migrate between the layers. From XRD the interlayer distances of the higher UPy content *f*-GO is larger, confirming the presence of functional groups between the layers. XPS is a surface technique so is unable to detect the interlayer chemistry of the GO.UPy samples. The <sup>13</sup>C MAS NMR data confirmed the reactivity of the hydroxyl groups, detected by XPS and, are most likely to be concentrated on the edges of the GO. As a result, the formation of the C-N bond is detected at all loadings due to its permanent positioning on the edges of the *f*-GO. At high UPy loading, the N-H bonds present in the UPy structure cannot be detected as they migrate between the *f*-GO layers

following dimerization and consequently, the ratio of detected C-N increases as the volume of N-H that can be detected is reduced.

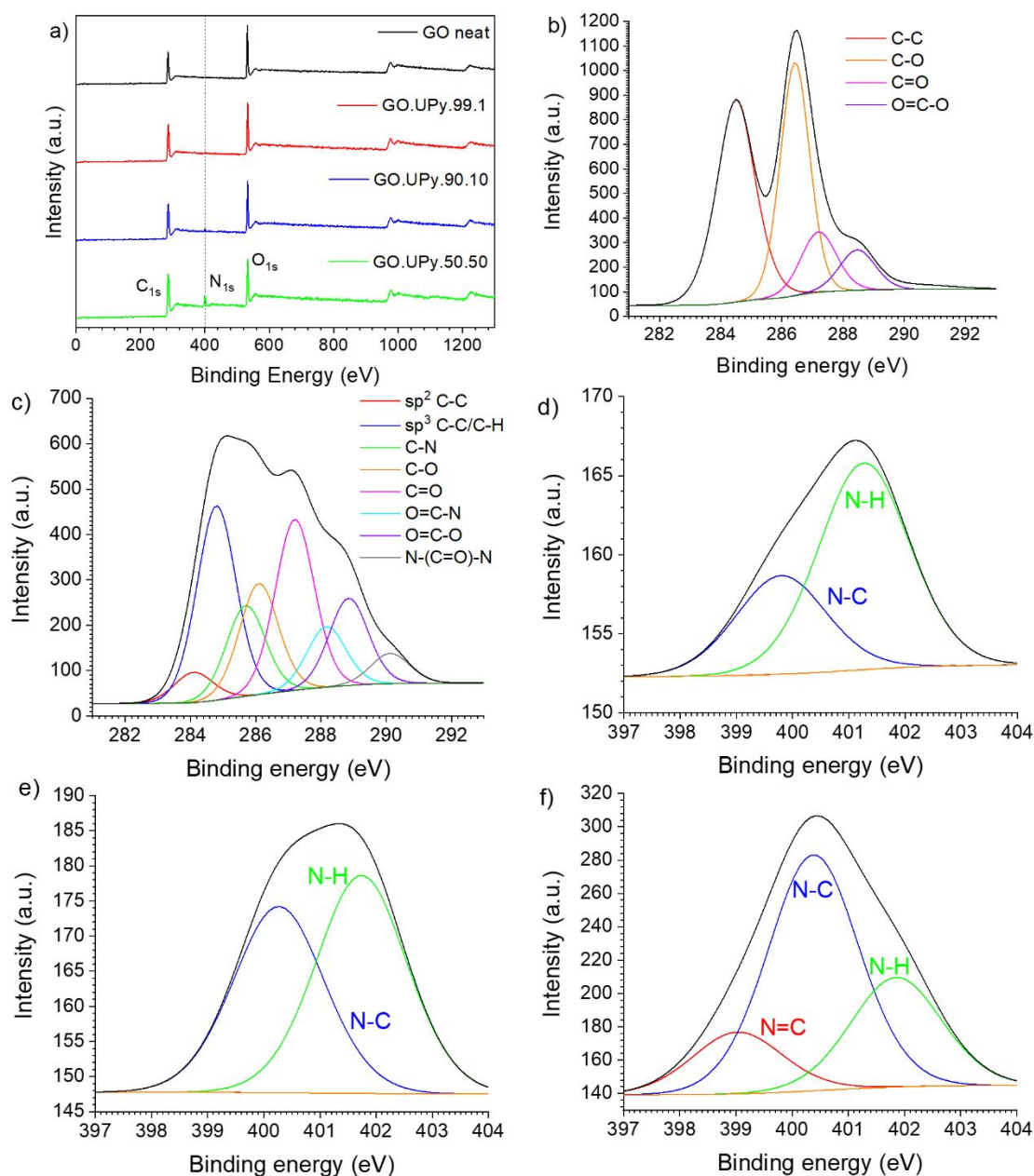
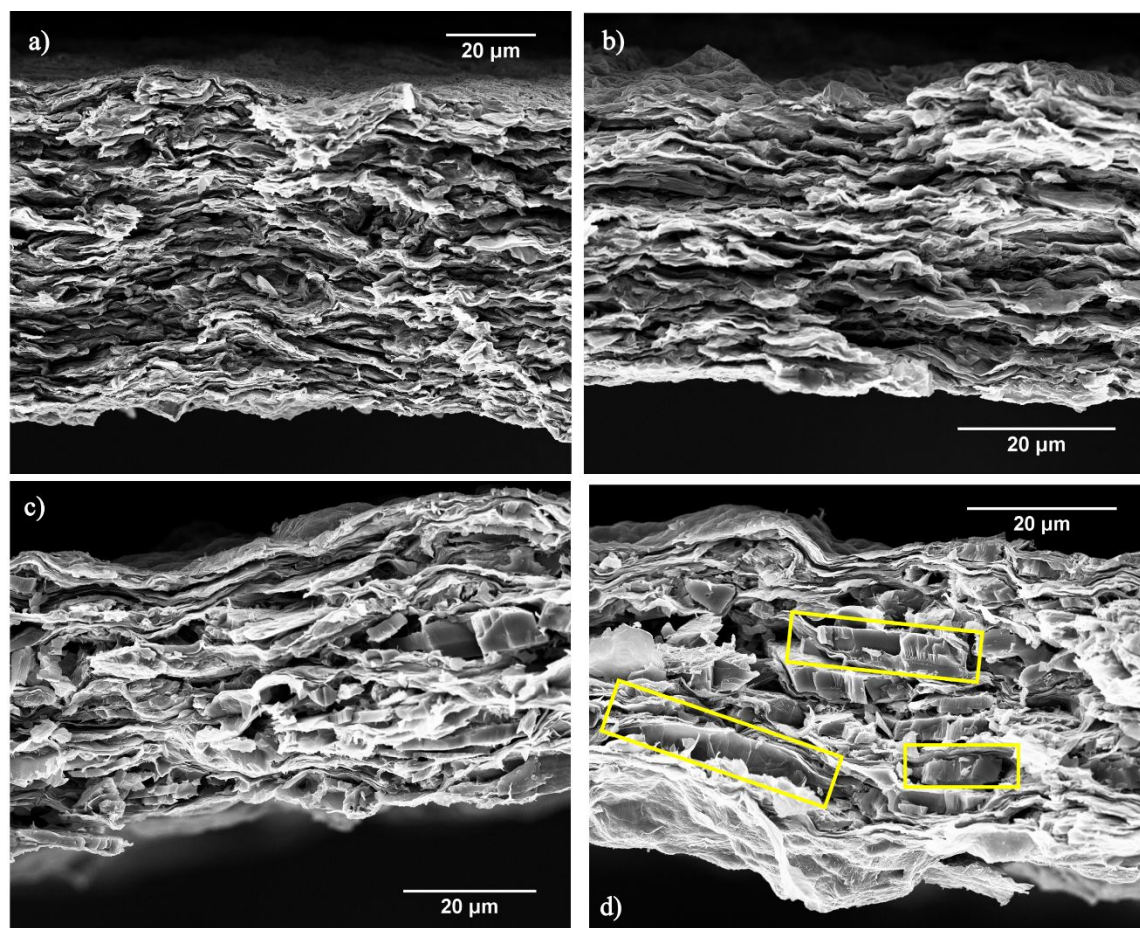


**Figure 4.** a) Survey spectra and b)-f) de-convoluted XPS spectra for GO and GO.UPy samples, b) C<sub>1s</sub> spectrum for neat GO, c) C<sub>1s</sub> spectrum for GO.UPy.50.50, d) N<sub>1s</sub> spectrum for GO.UPy.99.1, e) N<sub>1s</sub> spectrum for GO.UPy.90.10 and f) N<sub>1s</sub> spectrum for GO.UPy.50.50.



Nacre-mimetic materials can be prepared using a number of methods.<sup>8, 10, 18, 30</sup> The functionalised GO produced in this work was found only to be stable as a dispersion in DMSO following testing in a range of solvents (Table S2). Due to the high boiling point and low room-temperature volatility of DMSO, techniques such as solvent casting are not viable without long drying times or the application of high temperature. As a result, the dispersions of GO.UPy in DMSO were filtered through a hydrophilic PTFE membrane under vacuum. This technique has been widely used in the literature previously and proven to be effective at producing nacre-mimetic layered structures.<sup>18, 19, 31-33</sup> The stand alone nacre-like films produced were smooth and could be peeled with ease from the membrane (Figure S2).

SEM was used to image cross sections of the films produced (Figure 5). The unidirectional layered arrangement of the *f*-GO sheets is seen in each example thus, proving the nacre-mimetic structure of the films. It is interesting to observe the formation of larger 'brick-like' structures within the GO.UPy.50.50 material. These structures are most likely formed from the more densely packed highly functionalised GO, producing strongly bound groups of sheets. Once the filtration is completed, these structures self-assemble to form a layered structure due to the complementary interactions between the GO surface functional groups and those present on the rest of the *f*-GO sheets. This 'brick-like' structure is a result of high isocyanate content, as the same phenomena are not observed for the GO.UPy.99.1 and GO.UPy.90.10 films.



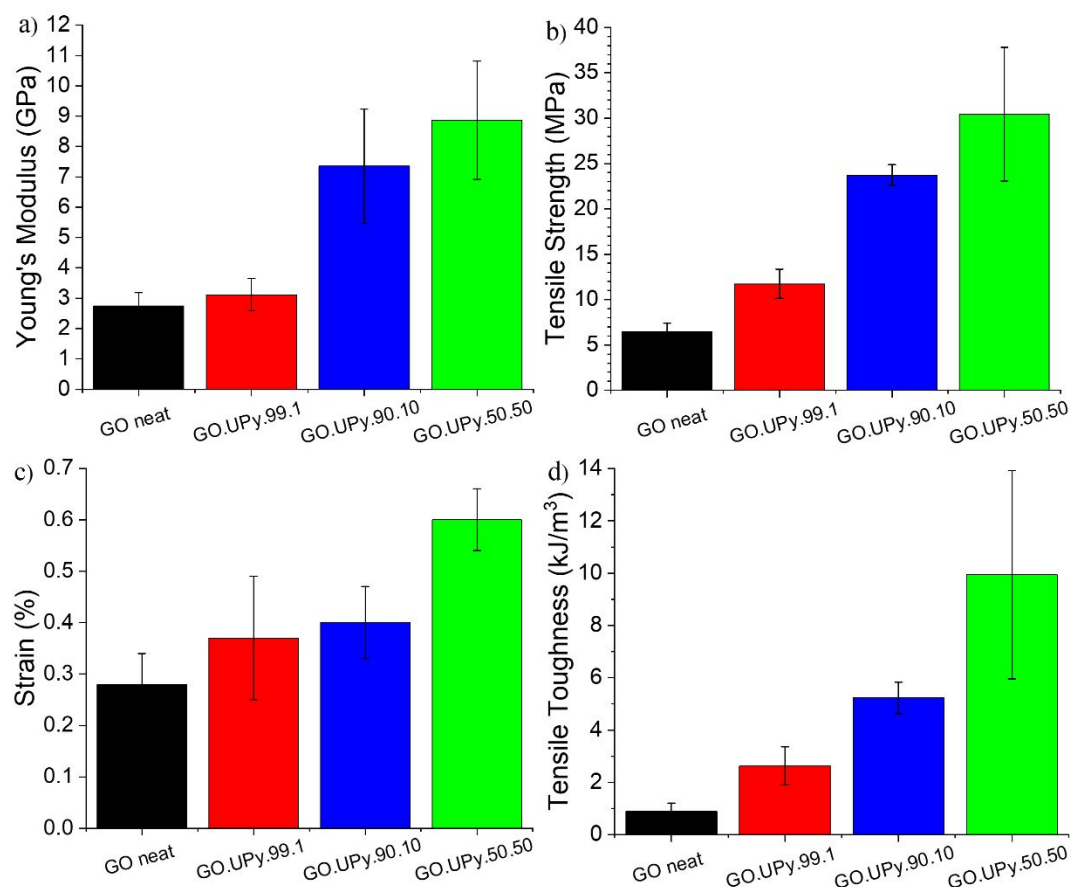
**Figure 5.** Cross-sectional SEM images of the GO.UPy films, a) GO.UPy.99.1, b) GO.UPy.90.10, c) GO.UPy.50.50 and d) GO.UPy.50.50 with examples of large ‘brick-like’ structures outlined in yellow.

Figure 2 b) shows the XRD spectra for GO and the GO.UPy ‘nacre-like’ films. For the neat GO film, a peak is obtained at  $2\theta = 9.48^\circ$  corresponding to an interlayer distance of 0.934 nm. This value is greater than that obtained for the same GO sample in powder form (0.816 nm) confirming the GO is packed more densely when in powder form. Upon reaction with 1 wt% UPy, the  $d$  spacing decreased to 0.921 nm where  $2\theta = 9.63^\circ$ . This effect is most likely due to the improved hydrogen bonding facilitated by the UPy group improving packing. Upon addition of higher isocyanate content, the interlayer distance increases. For GO.UPy.90.10,  $2\theta = 9.37^\circ$  corresponding to an interlayer distance of 0.943 nm and for GO.UPy.50.50,  $2\theta = 9.29^\circ$

corresponding to an interlayer distance of 0.959 nm. This suggests that for the lowest UPy concentration interlayer interactions increase and more dense packing of the *f*-GO sheets in the nacre-like film structure results. Upon addition of >10 wt% isocyanate, the steric effects of the bulky UPy group begin to outweigh any enhancement in interlayer interactions and forces the sheets to separate, hence larger *d*-spacing obtained. Indeed, for the GO.UPy.50.50 sample further peaks evolve, including at lower  $2\theta = 6.13^\circ$  corresponding to a *d* spacing of 1.44 nm, clear evidence the GO layers are further separated on addition of the highest UPy concentration. However, the interlayer spacing at around  $2\theta = 9.3^\circ$  for both GO.UPy.90.10 and GO.UPy.50.50 films are smaller than the equivalent samples when in powder form. Clearly, the presence of the 4 sites for hydrogen bonding in UPy (see Scheme 1) at higher loading promotes packing of the *f*-GO platelets when self-assembled in an unidirectional material. This behaviour is not observed for neat GO and GO.UPy.99.1 suggesting improved platelet packing in a random orientation. This is likely a result of the steric properties of the UPy group disrupting platelet packing, as the GO sheets are unable to align as effectively. When produced in an ordered arrangement (i.e. 'nacre-like' film), the UPy aids the self-assembly process and so promotes tighter platelet packing.

The tensile mechanical properties of the 'nacre-like' GO.UPy films were measured (Figure 6) and the Young's modulus (*E*), tensile strength ( $\sigma$ ), maximum strain and tensile toughness values determined and listed in Table S4. Overall, the reaction of UPy with GO has a positive effect on the mechanical properties of the stand-alone GO films. The improvements in tensile strength are expected due to the improved interlayer interactions facilitated by the 4-fold hydrogen bonding dimers. In traditional nacre-mimetic materials, the main failure mechanisms are platelet fracture or yielding of the soft interfaces.<sup>34</sup> The GO and GO.UPy films have no soft phase and so failure proceeds *via* platelet fracture or yielding at the interface between the platelet layers. By improving the interactions between the platelet layers, the

overall energy necessary to overcome interfacial interactions increases. As a result, the tensile strength of the GO nacre-like film increases significantly with increased UPy loading, by up to 470% compared with the neat GO film. The maximum strain also improves by a factor of two ( $\sim 2$ ) with the introduction of UPy, probably due to the structure of the UPy backbone. The six-carbon chain connecting the GO and the UPy groups (Figure S1) forms dimers (i.e. 12 carbon chains) and can extend and, unfold under applied load. This in turn allows the sheets to slide further over each other before reaching the extensibility of the UPy chains. Figure 7 provides a schematic illustration of our physical interpretation of the mechanism by which the mechanical properties of the stand-alone nacre-like GO.UPy films are enhanced relative, to the neat GO equivalent. With increasing concentration of UPy groups, the sliding of GO platelets is promoted and thus improving the maximum strain. The value of  $E$  also increases with increasing UPy concentration and follows a similar trend to both tensile strength and maximum strain. The  $E$  modulus is proportional to the ability of the matrix to transfer loads to the reinforcement via shear stresses. Here, the UPy plays the role of the matrix that enables load transfer to GO. This is the case when the UPy content is 10 and 50, but this mechanism is significantly reduced when the amount of GO is large ( $\sim 99$ ), or when there is only 'pure' GO platelets, i.e. no 'matrix' available to transfer the loads. Most interestingly there is an 1100% improvement in tensile toughness of the GO.UPy.50.50 film relative to the neat GO film. UPy functionalisation of GO resulted in a significant improvement in mechanical properties.



**Figure 6.** Tensile mechanical properties of nacre-like GO and GO.UPy films, a) Young's modulus, b) tensile strength, c) maximum strain and d) tensile toughness.

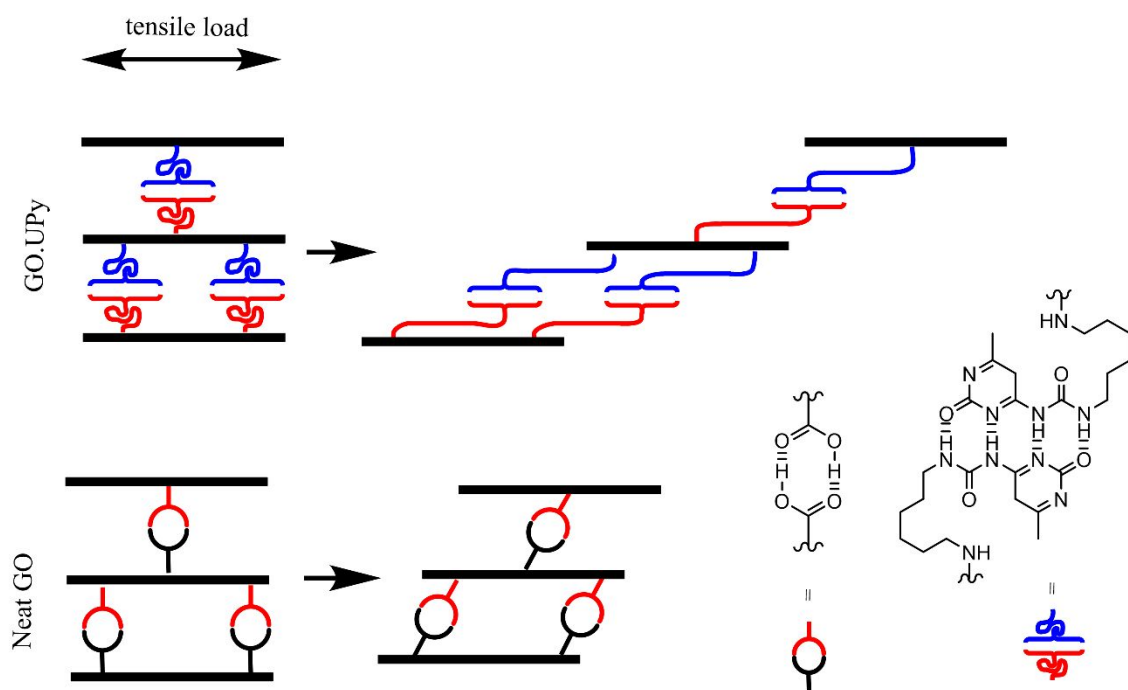


**Figure 7.** Schematic illustration of the improved extensibility observed for GO.UPy samples relative to neat GO.

Nacre-mimetic materials have been shown in the literature to offer enhanced gas barrier properties,<sup>17, 35, 36</sup> although the literature to date only describes the gas barrier properties of nacre-mimetic films that are typically supported on polymer films and, not as stand-alone films as in this study. The barrier properties of the GO and GO.UPy nacre-like films were tested for oxygen ( $O_2TR$ ), carbon dioxide ( $CO_2TR$ ) and water vapour transmission rate (WVTR), Figure 8, the corresponding gas barrier transmission curves are shown in Figure S3. To the best of our knowledge, there are no reports on the barrier properties of freestanding, polymer-free unidirectional 2D nanomaterial films in the literature. It can be seen that the functionalisation of GO with 1 wt% UPy has a beneficial effect on the barrier properties of the films for all the gases analysed. Upon addition of higher isocyanate content, the barrier performance decreases, and the gas transmission rate is higher than that for the neat GO film, as expected. The

interlayer spacing (XRD) between platelets is greater with increasing concentration of UPy groups, so the barrier to gas diffusion is less tortuous. Gas barrier properties strongly depend on the tortuosity of the pathway the gases must travel to permeate through the film.<sup>37</sup> An increase in interlayer spacing will increase the volume of the pathway and as a result reduce the resistance to diffusion during permeation.

Interestingly, the WVTR for the GO.UPy.50.50 film is less than that for GO.UPy.90.10, behaviour associated with the binding of water molecules by the UPy. The four sites for hydrogen bonding on UPy are able to bind to water molecules, preventing them from permeating, as UPy dimers can readily dissociate and exchange with water.<sup>38</sup> The dissociated UPy group can hydrogen bond with the water during transmission and slow the permeation rate through the film. The neat GO film has reduced hydrogen-bonding potential (i.e. no UPy) but the interlayer distances are smaller and this is more dominant than water capture by the UPy. As the interlayer spacing is the smallest for the GO.UPy.99.1 film, it has the most tortuous pathway for the water to permeate. This, combined with a small potential for water capture, results in this film being the best barrier of the four compositions. GO.UPy.90.10 and GO.UPy.50.50 have larger interlayer distances that results in an increase in water transmission when compared to GO and GO.UPy.99.1. The potential for water capture is higher in these materials. Water capture predominates over the reduction in the tortuous pathway at high UPy loading and thus results in improved barrier performance for GO.UPy.50.50.

The O<sub>2</sub>TR and CO<sub>2</sub>TR observed for these films are significantly lower than GO based nacre-mimetic films that include a polymer phase.<sup>36, 39</sup> The WVTR is also lower than that reported for other nacre-mimetic materials in the literature.<sup>40</sup> This could be explained by an increase in porosity as reported by Medina *et al.*<sup>41</sup> for other 2D nanomaterials. Using weight/volume calculations, the authors were able to determine that a 100 wt% nanoclay material was significantly more porous than the same nanoclay with 20 wt% or more polymer

content. The porosity was due to imperfect nanoplatelet stacking resulting in ‘pile-up’ and ultimately holes or voids in the structure. It is likely this phenomenon is also present in these nacre-like GO and GO.UPy samples. An increase in porosity will dramatically reduce the brick-wall effect, creating routes for the gas to penetrate and permeate through the film.

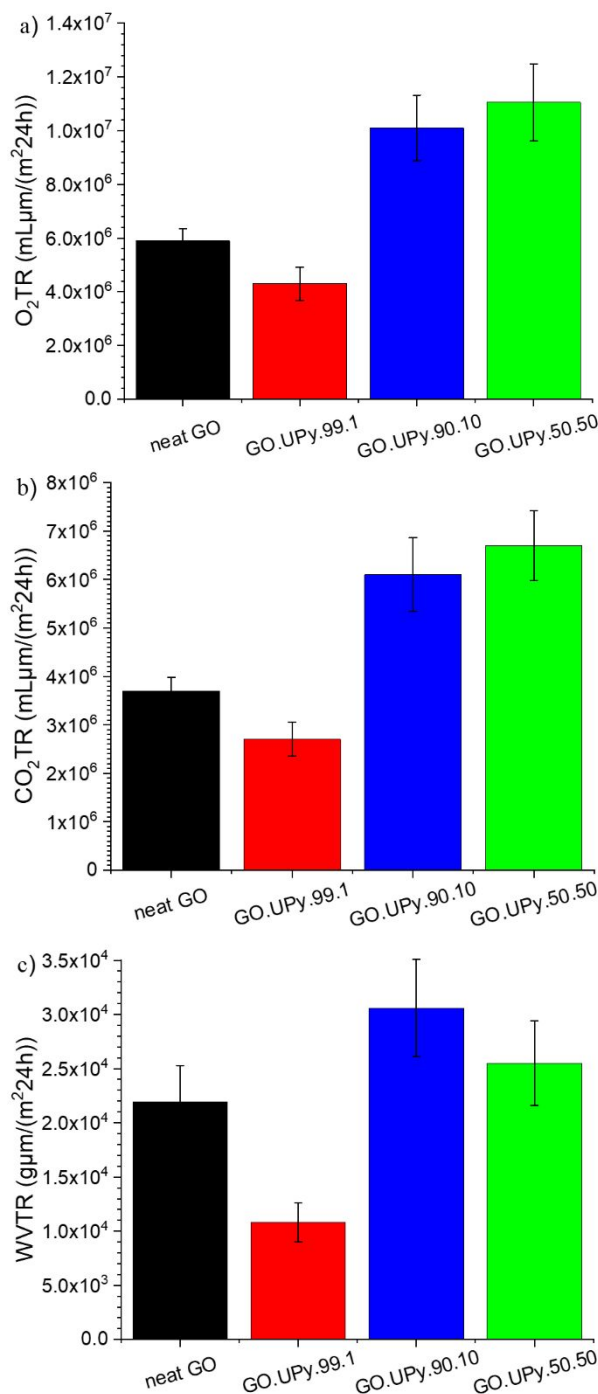


**Figure 8.** Barrier properties of GO and GO.UPy films towards different gases, a) oxygen transmission, b)  $CO_2$  transmission and c) water vapour transmission rate.



#### 4. Conclusions

The facile reaction of GO with UPy yielded a functionalised GO (*f*-GO) species which was used to produce freestanding ‘nacre-like’ films using a vacuum filtration process. The binding of UPy to GO was confirmed through the shift in the C=O stretch in the FTIR spectrum, shifts in the GO D and G bands in the Raman spectra, changes in elemental composition determined from XPS measurements and from the changes in the hydroxyl and epoxide peak intensities in solid state NMR studies of the GO.UPy materials. The uni-directional layered morphology of the nacre-like films was observed from cross-sectional SEM imaging. The spacing between GO layers increased with increasing UPy content resulting in the films becoming more porous. The barrier properties of the freestanding GO.UPy films to O<sub>2</sub> and CO<sub>2</sub> are determined by the tortuosity of the permeation pathways only, whilst H<sub>2</sub>O transmission is also retarded due to disassociation of UPy and exchange with water. The increased interfacial interactions, via UPy hydrogen bonding sites, between *f*-GO platelets resulted in a significant increase in the tensile strength (470%), tensile toughness (1100%) and by a factor of two the maximum strain of the GO nacre-like films. The increase in maximum strain is derived from, the ability of the platelets to slide more before failure via hydrogen bonding between UPy molecules. This work has demonstrated the potential for nacre-like materials making use of similar hydrogen bonded *f*-GO species.

#### Conflict of Interest

The authors report no conflicts of interest.

## Acknowledgements

A.S. thanks the EPSRC and Jaguar-Land Rover for funding an iCASE Award. N.L.K. thanks the EPSRC for funding a PhD studentship through the EPSRC Centre for Doctoral Training in Molecular Analytical Science (EP/L015307/1). J.V.H. acknowledges financial support for the solid state NMR instrumentation at Warwick used in this research which was funded by EPSRC (grants EP/M028186/1 and EP/K024418/1), the University of Warwick, and the Birmingham Science City AM1 and AM2 projects which were supported by Advantage West Midlands (AWM) and the European Regional Development Fund (ERDF).

## References

- (1) Abbas, S. S.; Rees, G. J.; Kelly, N. L.; Dancer, C. E. J.; Hanna, J. V.; McNally, T., Facile Silane Functionalization of Graphene Oxide. *Nanoscale* 2018, 10 (34), 16231-16242.
- (2) Song, Y.; Gao, Y.; Rong, H.; Wen, H.; Sha, Y.; Zhang, H.; Liu, H.-J.; Liu, Q., Functionalization of Graphene Oxide with Naphthalenediimide Diamine for High-performance Cathode Materials of Lithium-ion Batteries. *Sustainable Energy & Fuels* 2018, 2 (4), 803-810.
- (3) Wu, J.; Huang, G.; Li, H.; Wu, S.; Liu, Y.; Zheng, J., Enhanced Mechanical and Gas Barrier Properties of Rubber Nanocomposites with Surface Functionalized Graphene Oxide at Low Content. *Polymer* 2013, 54 (7), 1930-1937.
- (4) Stankovich, S.; Piner, R. D.; Nguyen, S. T.; Ruoff, R. S., Synthesis and Exfoliation of Isocyanate-treated Graphene Oxide Nanoplatelets. *Carbon* 2006, 44 (15), 3342-3347.
- (5) Zhao, H.; Wu, L.; Zhou, Z.; Zhang, L.; Chen, H., Improving the Antifouling Property of Polysulfone Ultrafiltration Membrane by Incorporation of Isocyanate-treated Graphene Oxide. *Physical Chemistry Chemical Physics* 2013, 15 (23), 9084-92.

- (6) Dong, Z.; Wang, D.; Liu, X.; Pei, X.; Chen, L.; Jin, J., Bio-inspired Surface-functionalization of Graphene Oxide for the Adsorption of Organic Dyes and Heavy Metal Ions with a Superhigh Capacity. *Journal of Materials Chemistry A* 2014, 2 (14), 5034-5040.
- (7) Igbinigun, E.; Fennell, Y.; Malaisamy, R.; Jones, K. L.; Morris, V., Graphene Oxide Functionalized Polyethersulfone Membrane to Reduce Organic Fouling. *Journal of Membrane Science* 2016, 514, 518-526.
- (8) Cui, W.; Li, M.; Liu, J.; Wang, B.; Zhang, C.; Jiang, L.; Cheng, Q., A Strong Integrated Strength and Toughness Artificial Nacre Based on Dopamine Cross-Linked Graphene Oxide. *ACS Nano* 2014, 8 (9), 9511-9517.
- (9) Wan, S.; Peng, J.; Li, Y.; Hu, H.; Jiang, L.; Cheng, Q., Use of Synergistic Interaction to Fabricate Strong, Tough and Conductive Artificial Nacre Based on Graphene Oxide and Chitosan. *ACS Nano* 2015, 9 (10), 9830-9836.
- (10) Wang, Y.; Li, T.; Ma, P.; Zhang, S.; Zhang, H.; Du, M.; Xie, Y.; Chen, M.; Dong, W.; Ming, W., Artificial Nacre from Supramolecular Assembly of Graphene Oxide. *ACS Nano* 2018, 12 (6), 6228-6235.
- (11) Xie, W.; Tadepalli, S.; Park, S. H.; Kazemi-Moridani, A.; Jiang, Q.; Singamaneni, S.; Lee, J. H., Extreme Mechanical Behavior of Nacre-Mimetic Graphene-Oxide and Silk Nanocomposites. *Nano Letters* 2018, 18 (2), 987-993.
- (12) Jackson, A. P.; Vincent, J. F.; Turner, R. M., The Mechanical Design of Nacre. *Proceedings of the Royal Society of London B* 1988, 234, 415-440.
- (13) Smith, B. L.; Schaffer, T. E.; Viani, M.; Thompson, J. B.; Frederick, N. A.; Kindt, J.; Belcher, A.; Stucky, G. D.; Morse, D. E.; Hansma, P. K., Molecular Mechanistic Origin of the Toughness of Natural Adhesives, Fibres and Composites. *Nature* 1999, 399, 761-763.
- (14) Li, L.; Ortiz, C., Pervasive Nanoscale Deformation Twinning as a Catalyst for Efficient Energy Dissipation in a Bioceramic Armour. *Nature Materials* 2014, 13 (5), 501-7.

- (15) Cheng, Q.; Wu, M.; Li, M.; Jiang, L.; Tang, Z., Ultratough artificial nacre based on conjugated cross-linked graphene oxide. *Angewandte Chemie International Edition England* 2013, 52 (13), 3750-5.
- (16) Putz, K. W.; Compton, O. C.; Palmeri, M. J.; Nguyen, S. T.; Brinson, L. C., High-Nanofiller-Content Graphene Oxide-Polymer Nanocomposites via Vacuum-Assisted Self-Assembly. *Advanced Functional Materials* 2010, 20 (19), 3322-3329.
- (17) Shahzadi, K.; Mohsin, I.; Wu, L.; Ge, X.; Jiang, Y.; Li, H.; Mu, X., Bio-Based Artificial Nacre with Excellent Mechanical and Barrier Properties Realized by a Facile In Situ Reduction and Cross-Linking Reaction. *ACS Nano* 2017, 11 (1), 325-334.
- (18) Wan, S.; Xu, F.; Jiang, L.; Cheng, Q., Superior Fatigue Resistant Bioinspired Graphene-Based Nanocomposite via Synergistic Interfacial Interactions. *Advanced Functional Materials* 2017, 27 (10), 1605636.
- (19) Park, S.; Lee, K.-S.; Bozoklu, G.; Cai, W.; Nguyen, S. T.; Ruoff, R. S., Graphene Oxide Papers Modified by Divalent Ions-Enhancing Mechanical Properties via Chemical Cross-Linking. *ACS Nano* 2008, 2 (3), 572-578.
- (20) Harris, R. K.; Becker, E. D.; Cabral de Menezes, S. M.; Goodfellow, R.; Granger, P., NMR Nomenclature: Nuclear Spin Properties and Conventions for Chemical Shifts. IUPAC Recommendations 2001. *Solid State Nuclear Magnetic Resonance* 2002, 22 (4), 458-483.
- (21) Kim, F.; Cote, L. J.; Huang, J., Graphene Oxide: Surface Activity and Two-Dimensional Assembly. *Advanced Materials* 2010, 22 (17), 1954-8.
- (22) Blagbrough, I. S.; MacKenzie, N. E.; Ortiz, C.; Scott, A. I., The Condensation Reaction between Isocyanates and Carboxylic Acids: A Practical Synthesis of Substituted Amides and Anilides. *Tetrahedron Letters* 1986, 27 (11), 1251-1254.
- (23) Gürtler, C.; Danielmeier, K., A Catalyst System for the Reaction of Carboxylic Acids with Aliphatic Isocyanates. *Tetrahedron Letters* 2004, 45 (12), 2515-2521.

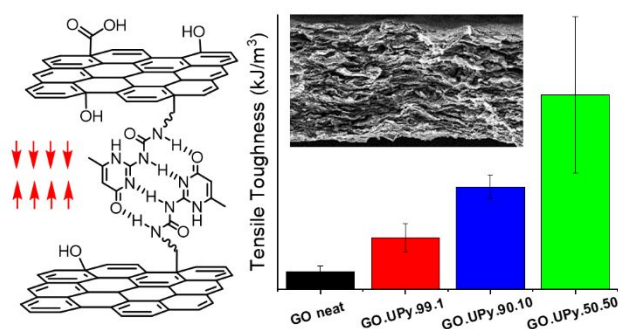
- (24) DeMeuse, M. T.; Gillham, J. K.; Parodi, F., Evolution of Properties of an Isocyanate/Epoxy Thermosetting System During Cure: Continuous Heating (CHT) and Isothermal Time-Temperature-Transformation (TTT) Cure Diagrams. *Journal of Applied Polymer Science* 1996, 64 (1), 15-25.
- (25) Viinikanoja, A.; Kauppila, J.; Damlin, P.; Suominen, M.; Kvarnstrom, C., In-situ FTIR and Raman Spectroelectrochemical Characterization of Graphene Oxide upon Electrochemical Reduction in Organic Solvents. *Physical Chemistry Chemical Physics* 2015, 17 (18), 12115-23.
- (26) Childres, I.; Jauregui, L. A.; Park, W.; Cao, H.; Chen, Y. P., Raman Spectroscopy of Graphene and Related Materials. In *New Developments in Photon and Materials Research*, Jang, J. I., Ed. Nova Science Publishers: 2013; pp 403-418.
- (27) Park, S.; Hu, Y.; Hwang, J. O.; Lee, E. S.; Casabianca, L. B.; Cai, W.; Potts, J. R.; Ha, H. W.; Chen, S.; Oh, J.; Kim, S. O.; Kim, Y. H.; Ishii, Y.; Ruoff, R. S., Chemical Structures of Hydrazine-treated Graphene Oxide and Generation of Aromatic Nitrogen Doping. *Nature Communications* 2012, 3, 638.
- (28) Thomas, H. R.; Day, S. P.; Woodruff, W. E.; Vallés, C.; Young, R. J.; Kinloch, I. A.; Morley, G. W.; Hanna, J. V.; Wilson, N. R.; Rourke, J. P., Deoxygenation of Graphene Oxide: Reduction or Cleaning? *Chemistry of Materials* 2013, 25 (18), 3580-3588.
- (29) Yap, P. L.; Kabiri, S.; Tran, D. N. H.; Losic, D., Multifunctional Binding Chemistry on Modified Graphene Composite for Selective and Highly Efficient Adsorption of Mercury. *ACS Applied Materials and Interfaces* 2019, 11 (6), 6350-6362.
- (30) Liu, Y.; Shi, X.; Liu, S.; Li, H.; Zhang, H.; Wang, C.; Liang, J.; Chen, Y., Biomimetic Printable Nanocomposite for Healable, Ultrasensitive, Stretchable and Ultradurable Strain Sensor. *Nano Energy* 2019, 63, 103898.

- (31) Gao, Y.; Liu, L.-Q.; Zu, S.-Z.; Peng, K.; Zhou, D.; Han, B.-H.; Zhang, Z., The Effect of Interlayer Adhesion on the Mechanical Behaviours of Macroscopic Graphene Oxide Papers. ACS Nano 2011, 5 (3), 2134-2141.
- (32) Hu, K.; Tolentino, L. S.; Kulkarni, D. D.; Ye, C.; Kumar, S.; Tsukruk, V. V., Written-in Conductive Patterns on Robust Graphene Oxide Biopaper by Electrochemical Microstamping. Angewandte Chemie International Edition England 2013, 52 (51), 13784-8.
- (33) Chen, K.; Tang, X.; Yue, Y.; Zhao, H.; Guo, L., Strong and Tough Layered Nanocomposites with Buried Interfaces. ACS Nano 2016, 10 (4), 4816-27.
- (34) Barthelat, F.; Rabiei, R., Toughness Amplification in Natural Composites. Journal of the Mechanics and Physics of Solids 2011, 59 (4), 829-840.
- (35) Song, Y.; Gerringer, J.; Qin, S.; Grunlan, J. C., High Oxygen Barrier Thin Film from Aqueous Polymer/Clay Slurry. Industrial & Engineering Chemistry Research 2018, 57 (20), 6904-6909.
- (36) Yang, Y. H.; Bolling, L.; Priolo, M. A.; Grunlan, J. C., Super Gas Barrier and Selectivity of Graphene Oxide-Polymer Multilayer Thin Films. Advanced Materials 2013, 25 (4), 503-8.
- (37) Feldman, D., Polymer Nanocomposite Barriers. Journal of Macromolecular Science, Part A 2013, 50 (4), 441-448.
- (38) Söntjens, S. H. M.; Sijbesma, R. P.; van der Genderen, M. H. P.; Meijer, E. W., Stability and Lifetime of Quandruply Hydrogen Bonded 2-Uriedo-4[1*H*]-pyrimidinone Dimers. Journal of the American Chemical Society 2000, 122, 7847-7493.
- (39) Chen, J. T.; Fu, Y. J.; An, Q. F.; Lo, S. C.; Huang, S. H.; Hung, W. S.; Hu, C. C.; Lee, K. R.; Lai, J. Y., Tuning Nanostructure of Graphene Oxide/Polyelectrolyte LbL Assemblies by Controlling pH of GO Suspension to Fabricate Transparent and Super Gas Barrier Films. Nanoscale 2013, 5 (19), 9081-8.

(40) Ding, F.; Liu, J.; Zeng, S.; Xia, Y.; Wells, K. M.; Nieh, M.-P.; Sun, L., Biomimetic Nanocoatings With Exceptional Mechanical Barrier, and Flame-Retardant Properties from Large-scale One-step Coassembly. *Science Advances* 2017, 3, 1-9.

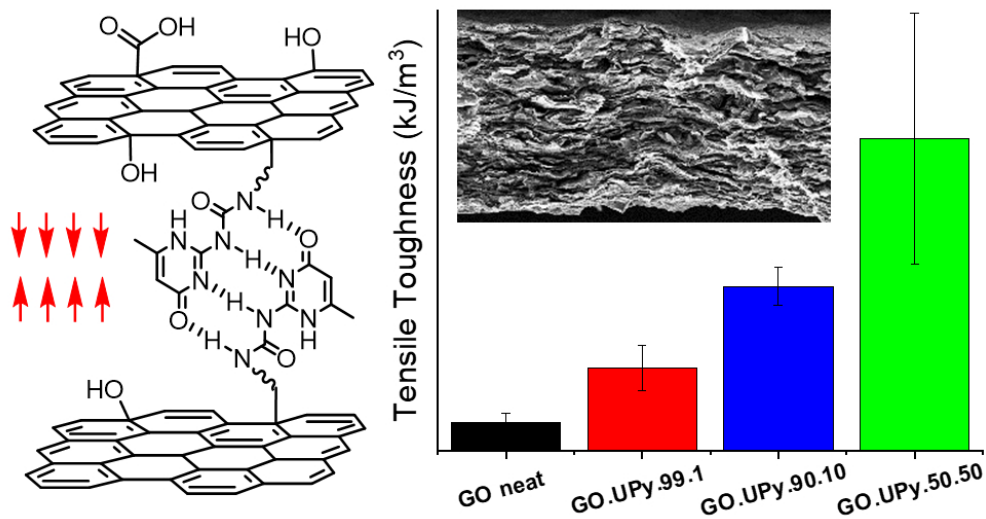
(41) Medina, L.; Nishiyama, Y.; Daicho, K.; Saito, T.; Yan, M.; Berglund, L. A., Nanostructure and Properties of Nacre-Inspired Clay/Cellulose Nanocomposites—Synchrotron X-ray Scattering Analysis. *Macromolecules* 2019, 52 (8), 3131-3140.

FOR TABLE OF CONTENTS ONLY:



Supplementary Information:

- Isocyanate – carboxylic acid/hydroxyl/epoxide reaction mechanisms; elemental composition data for GO and GO.UPy samples; digital photographs of GO/GO.UPy films; gas-barrier transmission curves; dispersion experiments of GO.UPy powders; SSNMR assignments; tabulated mechanical tensile properties.



82x44mm (300 x 300 DPI)